Application of the partial-Fourier-transform approach for tunnel ionization of molecules

Mingming Liu[1] and Yunquan Liu[1,2]
[1]*Department of Physics and State Key Laboratory for Mesoscopic Physics, Peking University, Beijing 100871, China*
[2]*Collaborative Innovation Center of Quantum Matter, Beijing 100871, China*
(Received 3 March 2016; published 29 April 2016)

Combining the partial-Fourier-transform approach with Wenzel-Kramers-Brillouin approximation, we theoretically study the strong-field tunneling ionization of diatomic and polyatomic molecules. First we obtain the analytical expression of momentum distribution at the tunnel exit of diatomic molecules, and then we calculate the alignment-dependent ionization rate at different laser intensities and internuclear distances. We show that the internuclear distance has a significant effect on the alignment dependence of the ionization rate. Using this approach, we can also separate the contributions of each atomic center and show the interference effect between them. Finally, we extend this method to a polyatomic molecule, benzene, as an example.

DOI: 10.1103/PhysRevA.93.043426

I. INTRODUCTION

The tunneling of atoms and molecules is the foundation of attosecond science, which is the first step of the important three-step model [1]. A strong laser field suppresses the Coulomb potential, forming an instantaneous potential barrier. The bond electrons can be freed by tunneling and then will oscillate in the laser field. A fraction of the tunneled electrons can be driven back to its parent ion, then scatter off it, or recombine with it accompanied by the emission of a photon. In the last decade, the tunneling of molecules attracted a lot of attention, and several state-of-the-art attosecond techniques are based on it. In photoelectron tomography experiments [2], the tunneling of molecules determines the calibration of continuum wave packets, which will further influence the tomographic reconstruction of molecular orbitals. Part of the tunneling electrons are diffracted by molecular ions, and the diffraction pattern in photoelectron momentum distribution encodes information about molecular orbitals as reveled in laser-induced electron diffraction experiments [3–6]. While the tunneling of atoms has been studied thoroughly from the famous work of Keldysh [7] for more than 50 years [8–11], theoretical investigation of molecular tunneling is still ongoing. The most common approaches include molecular strong-field approximation (MO-SFA) [12–14] and molecular Ammosov-Delone-Krainov (MO-ADK) theory [15]. While both theories have achieved great success in describing experimental results, the former suffers from gauge noninvariance, and the latter does not include the effect of multicenter interference.

Recently, Murray *et al.* proposed a simple and straightforward method to study the tunneling of atoms [16]. The authors introduce the partial Fourier transform of field-free ground state wave function of atoms. With the help of this specific wave function, they reduce the three-dimensional tunneling problem to one dimension and utilize the results of Wentzel-Kramers-Brillouin (WKB) approximation directly. They successfully reproduce the ADK ionization rate for atoms and explain the alignment-dependent ionization rate of CO_2 [17].

In our work we present the application of the partial-Fourier-transform approach to the study of strong-field tunneling ionization of homonuclear diatomic molecules as well as polyatomic molecules. We represent the highest occupied molecular orbitals (HOMO) by linear combination of atomic orbitals and obtain the amplitude and phase structure of the tunneling wave packet at the tunnel exit analytically. The analytical expression of the tunneling wave packet at the tunnel exit is critical for the calibration of a continuum wave packet in tomographic experiments, and its phase structure has been demonstrated to have a significant effect on the alignment-dependent holography pattern of N_2 [18]. Thus our method will facilitate the study of various molecular imaging approaches. Different from MO-ADK theory, utilizing the two-center expression of the HOMO of diatomic molecules, we separate the contributions of each atomic center and show the interference between them explicitly. This approach can also be straightforwardly extended to polyatomic molecules.

In Sec. II of this paper, we present the derivation of the tunneling wave packet of homonuclear diatomic molecules. Then we show the results of H_2 in Sec. III and O_2 in Sec. IV. In Sec. V we extend this method to a polyatomic molecule, benzene. Finally, we give the conclusions in Sec. VI.

II. TUNNELING THEORY FOR HOMONUCLEAR DIATOMIC MOLECULES

First we introduce the partial-Fourier-transform method for atoms briefly. We consider the situation of zero range potential and a static electric field, as shown in Fig. 1(a). The Hamiltonian in length gauge of this system is

$$\hat{H} = \frac{\hat{\mathbf{p}}^2}{2} - Fz. \tag{1}$$

Here F is the strength of electric field, which points towards the minus z axis. The atomic wave function in mixed representation is

$$\Phi_{\text{atom}}(p_x, p_y, z) = \frac{1}{2\pi} \iint dx\, dy\, e^{-ixp_x - iyp_y} \Psi_{\text{atom}}(x, y, z). \tag{2}$$

Here the wave function is represented by two momentum variables perpendicular to the polarization axis, as well as one coordinate variable parallel to the polarization axis. With the help of this specific expression, we can simplify the

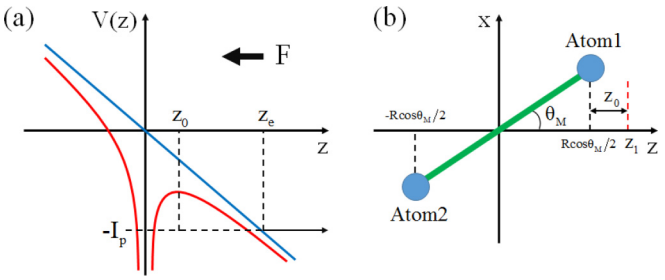

FIG. 1. (a) The sketch of the ionization of atoms in static electric field. The thick black arrow indicates the direction of the static electric field. The straight blue line represents the potential induced by the static electric field, while the bent red line includes the Coulomb potential. The vertical dashed line indicates the positions of tunnel exit z_e and matching point z_0 (see text). (b) The configuration of a diatomic molecule. The thick green line represents the molecular axis. The static electric field points towards minus z direction. The alignment angle is θ_M. The longitudinal displacement is $R\cos\theta_M/2$ for atom 1 and $-R\cos\theta_M/2$ for atom 2. The dashed red line indicates the position of the new matching point for atom 1.

three-dimensional Schrödinger equation as follows:

$$-\frac{\partial^2\Phi_{\rm atom}(p_x,p_y,z)}{\partial z^2}=2(E'+Fz)\Phi_{\rm atom}(p_x,p_y,z). \quad (3)$$

Here $E'=-(I_p+p_x^2/2+p_y^2/2)$, and I_p is the ionization potential. Then we can utilize the technique of one-dimensional WKB approximation. According to WKB approximation, the wave function should take the form of

$$\Phi_{\rm atom}(p_x,p_y,z)=\frac{C}{\sqrt{p_z(z)}}\exp[iS(p_x,p_y,z)]. \quad (4)$$

Here $S(p_x,p_y,z)$ is the classical action, and $p_z(z)=|\partial S(p_x,p_y,z)/\partial z|$ is the kinetic momentum along the polarization axis. Then we find a point z_0 in the classically forbidden region where $z_0\gg 1$ so that we can adopt the asymptotic form of field-free wave function, and $z_0\ll z_e$ ($z_e=I_p/F$ is the tunnel exit) so that the laser field is still small compared with Coulomb potential. At this point the WKB solution should match with the field-free wave function. The constant C in Eq. (4) can be determined by this matching procedure and the wave function at tunnel exit is given by

$$\begin{aligned}&\Phi_{\rm atom}(p_x,p_y,z\to z_e)\\&=\Phi_{\rm atom}(p_x,p_y,z_0)\sqrt{\frac{\kappa}{p_z(z)}}\\&\quad\times\exp\{i[S(p_x,p_y,z)-S(p_x,p_y,z_0)]\}.\end{aligned} \quad (5)$$

Here $\Phi_{\rm atom}(p_x,p_y,z_0)$ is the field-free wave function at matching point, and $\kappa=\sqrt{2I_p}$. Note that WKB approximation is not applicable right at the tunnel exit. The expression in Eq. (5) is applicable for some point just beyond the tunnel exit. In the following paragraphs we will omit the notation $z\to z_e$. The expression in Eq. (5) also represents the transverse momentum distribution at the tunnel exit.

We start from the treatment of homonuclear diatomic molecules using the partial-Fourier-transform approach. The HOMO of a homonuclear diatomic molecule is the superposition of two atomic orbitals, one at each atomic center,

$$\begin{aligned}\Psi_{\rm molecule}(\mathbf{r})=&\frac{1}{\sqrt{2\pm 2S_{\rm OI}}}[\Psi_{\rm atom1}(\mathbf{r}-\mathbf{R}/2)\\&\pm\Psi_{\rm atom2}(\mathbf{r}+\mathbf{R}/2)].\end{aligned} \quad (6)$$

Here $\mathbf{R}$ points from one atomic center to the other, and $S_{\rm OI}$ is the overlap integral. The positive sign in Eq. (6) represents the bonding orbital, and the negative sign the antibonding orbital. In the following paragraphs we will neglect the coefficient before the square brackets in Eq. (6), which is of no physical significance when calculating the relative ionization rate. The partial Fourier transform of this molecular orbital is

$$\begin{aligned}\Phi_{\rm molecule}(p_x,p_y,z)=&\exp(-ip_xR\sin\theta_M\cos\varphi_M/2-ip_yR\sin\theta_M\sin\varphi_M/2)\Phi_{\rm atom1}(p_x,p_y,z-R\cos\theta_M/2)\\&\pm\exp(ip_xR\sin\theta_M\cos\varphi_M/2+ip_yR\sin\theta_M\sin\varphi_M/2)\Phi_{\rm atom2}(p_x,p_y,z+R\cos\theta_M/2).\end{aligned} \quad (7)$$

Here θ_M and φ_M are the polar and azimuthal angles of the molecular axis, respectively. From Eq. (7) the wave function in mixed representation of a homonuclear diatomic molecule is also the superposition of two atomic components, but the contribution of each atom is multiplied by a phase factor, which originates from the transverse displacement from the molecular center perpendicular to the electric field. Because of the longitudinal displacement parallel to the electric field, the atomic contributions $\Phi_{\rm atom1}$ and $\Phi_{\rm Atom2}$ are different from the original expression in Eq. (5). We take atom 1, for example, to elucidate the derivation of these contributions. As there is a longitudinal displacement, the matching point of each atom will move accordingly. The longitudinal displacement of atom 1 is $R\cos\theta_M/2$, and thus we assume the new matching point is $z_1=z_0+R\cos\theta_M/2$, then the wave function in mixed representation is

$$\Phi_{\rm atom1}(p_x,p_y,z_e-R\cos\theta_M/2)=\Phi_{\rm atom1}(p_x,p_y,z_1-R\cos\theta_M/2)\sqrt{\frac{\kappa}{p_z(z_e)}}\exp\{i[S(p_x,p_y,z_e)-S(p_x,p_y,z_1)]\}. \quad (8)$$

Under the condition that $z_1\ll z_e$ we can expand the exponential term in Eq. (8) in powers of z_1 up to the first order,

$$\Phi_{\rm atom1}(p_x,p_y,z_e-R\cos\theta_M/2)=\Phi_{\rm atom}(p_x,p_y,z_0)\sqrt{\frac{\kappa}{p_z(z_e)}}\exp\left(-\frac{\kappa^3}{3F}-\frac{\kappa p_\perp^2}{2F}+\kappa z_0+\kappa R\cos\theta_M/2\right). \quad (9)$$

Here $p_\perp=\sqrt{p_x^2+p_y^2}$. We can see that the exponential term is modified by $\kappa R\cos\theta_M/2$, which originates from the longitudinal displacement and gives the relative weight of two atomic contributions. The treatment of atom 2 is similar. The modification of

relative weight is easy to understand. For the specific configuration in Fig. 1(b), the potential barrier which electrons from atom 1 are going to penetrate is narrower than that for atom 2, so the probability that electrons penetrate the potential barrier from atom 1 is bigger than that from atom 2. After inserting these atomic terms into Eq. (7) and including the Coulomb correction under the barrier [16,19], we get the expression in mixed representation for homonuclear diatomic molecules,

$$\Phi_{\text{molecule}}(p_x,p_y,z_e)=\left\{\begin{matrix}\exp(-ip_xR\,\sin\theta_M\cos\varphi_M/2-ip_yR\,\sin\theta_M\sin\varphi_M/2)\exp(\kappa R\,\cos\theta_M/2)\\ \pm\exp(ip_xR\,\sin\theta_M\cos\varphi_M/2+ip_yR\,\sin\theta_M\sin\varphi_M/2)\exp(-\kappa R\cos\theta_M/2)\end{matrix}\right\}$$
$$\times\Phi_{\text{atom}}(p_x,p_y,z_0)\sqrt{\frac{\kappa}{p_z(z_e)}}\left(\frac{2\kappa^2}{Fz_0}\right)^{Q/\kappa}\exp\left(-\frac{\kappa^3}{3F}-\frac{\kappa p_\perp^2}{2F}+\kappa z_0\right) \tag{10}$$

Here Q is the charge of the molecular ion. In order to cancel the matching point in the final expression, we still use atomic potential when calculating the Coulomb correction under the barrier for each atomic contribution. The asymptotic form of atomic wave function is

$$\Psi_{\kappa lm}(\mathbf{r})=(-1)^{(m+|m|)/2}i^lC_{\kappa l}N_{lm}\kappa^{3/2}(\kappa r)^{Q/\kappa-1}e^{-\kappa r}P_l^{|m|}(\cos\theta)e^{im\varphi}. \tag{11}$$

Here,

$$N_{lm}=\sqrt{\frac{2l+1}{4\pi}\frac{(l-|m|)!}{(l+|m|)!}}. \tag{12}$$

The expression in mixed representation is

$$\Phi_{\kappa lm}(p_x,p_y,z)=i^{l-m}(-1)^{|m|}\frac{C_{\kappa l}N_{lm}}{2^{|m|}|m|!}\frac{(l+|m|)!}{(l-|m|)!}\kappa^{Q/\kappa-1/2}z^{Q/\kappa}e^{-\kappa z}\left(\frac{p_\perp}{\kappa}\right)^{|m|}e^{im\phi_0}. \tag{13}$$

Here ϕ_0 is the azimuthal angle of $p_\perp$. In the derivation of Eq. (13) we make the assumption that $p_\perp/\kappa\ll 1$. So far we have not considered the rotation of molecules. If the molecular axis rotates, the atomic orbitals constituting the molecular orbital will rotate accordingly. The rotated atomic orbitals can be represented as follows:

$$\Phi_{\kappa lm}(p_x,p_y,z)=\sum_{m'}D^l_{m'm}(\theta_M,\varphi_M,\gamma_M)i^{l-m'}(-1)^{|m'|}\frac{C_{\kappa l}N_{lm'}}{2^{|m'|}|m'|!}\frac{(l+|m'|)!}{(l-|m'|)!}\kappa^{Q/\kappa-1/2}z^{Q/\kappa}e^{-\kappa z}\left(\frac{p_\perp}{\kappa}\right)^{|m'|}e^{im'\phi_0}. \tag{14}$$

Here $D^l_{m'm}(\theta_M,\varphi_M,\gamma_M)$ is the rotation matrix, and γ_M specify the rotation around the molecular axis. After inserting Eq. (14) into Eq. (10), we get the final expression in mixed representation at the tunnel exit for a homonuclear diatomic molecule,

$$\Phi_{\text{molecule}}(p_x,p_y,z_e)=\left\{\begin{matrix}\exp(-ip_xR\,\sin\theta_M\cos\varphi_M/2-ip_yR\,\sin\theta_M\sin\varphi_M/2)\exp(\kappa R\,\cos\theta_M/2)\\ \pm\exp(ip_xR\,\sin\theta_M\cos\varphi_M/2+ip_yR\,\sin\theta_M\sin\varphi_M/2)\exp(-\kappa R\,\cos\theta_M/2)\end{matrix}\right\}$$
$$\times\sum_{m'}D^l_{m'm}(\theta_M,\varphi_M,\gamma_M)\frac{(i)^{l-m'}(-1)^{|m'|}}{\sqrt{p_z(z_e)}}\frac{C_{\kappa l}N_{lm'}}{2^{|m'|}|m'|!}\frac{(l+|m'|)!}{(l-|m'|)!}\left(\frac{p_\perp}{\kappa}\right)^{|m'|}e^{im'\phi_0}\left(\frac{2\kappa^3}{F}\right)^{Q/\kappa}$$
$$\times\exp\left(-\frac{\kappa^3}{3F}-\frac{\kappa p_\perp^2}{2F}\right) \tag{15}$$

From Eq. (15) we can see that the wave function in mixed representation is the one for atoms multiplied by a structural factor. The structural factor in the curly brackets in Eq. (15) depends on the orientation of the molecules, the distance between two atomic centers, and the transverse momentum at the tunnel exit. It reflects the effect of the structure of molecular orbital on the momentum distribution at tunnel exit. Finally, the ionization rate in the linearly polarized laser field can be given by the integral

$$\Gamma=\left(\frac{3F}{\pi\kappa^3}\right)^{1/2}\int dp_x\,dp_y\,p_z(z_e)|\Phi_{\text{molecule}}(p_x,p_y,z_e)|^2. \tag{16}$$

III. HYDROGEN

We take H_2, for example, to show the application of the partial-Fourier-transform approach. The HOMO of H_2 is $1\sigma_g$, and there is one $1s$ orbital at each atomic center. Because the $1s$ orbital is spherically symmetric, the sum in Eq. (15) is unnecessary. The corresponding wave function in mixed representation at tunnel exit is

$$\Phi_{H_2}(p_x,p_y,z_e)=\left\{\begin{matrix}\exp(-ip_xR\,\sin\theta_M\cos\varphi_M/2-ip_yR\,\sin\theta_M\sin\varphi_M/2)\exp(\kappa R\,\cos\theta_M/2)\\ +\exp(ip_xR\,\sin\theta_M\cos\varphi_M/2+ip_yR\,\sin\theta_M\sin\varphi_M/2)\exp(-\kappa R\,\cos\theta_M/2)\end{matrix}\right\}$$
$$\times\frac{C_{\kappa0}}{2\sqrt{\pi\,p_z(z_e)}}\left(\frac{2\kappa^3}{F}\right)^{Q/\kappa}\exp\left(-\frac{\kappa^3}{3F}-\frac{\kappa p_\perp^2}{2F}\right) \tag{17}$$

After inserting this expression into Eq. (16), we get the ionization rate at different alignment angles,

$$\Gamma_{H_2} = \frac{|C_{\kappa 0}|^2}{4\pi}\left(\frac{2\kappa^3}{F}\right)^{2Q/\kappa}\left(\frac{3F}{\pi\kappa^3}\right)^{1/2}\exp\left(-\frac{2\kappa^3}{3F}\right)$$
$$\times \iint dp_x\, dp_y[\exp(\kappa R\,\cos\theta_M) + \exp(-\kappa R\,\cos\theta_M) + 2\cos(p_y R\,\sin\theta_M)]\exp\left(-\frac{\kappa p_\perp^2}{F}\right) \quad (18)$$

In Fig. 2 we show the numerical results of Eq. (18). We neglect the constant $C_{\kappa 0}$, which is of no physical significance when calculating the relative ionization rate of homonuclear diatomic and polyatomic molecules. If the atomic orbitals constituting the HOMO are different, e.g., the case of heteronuclear diatomic molecules, this constant must be considered carefully. In Fig. 2(a), we show the alignment dependence of the ionization rate at different laser intensities. We can see that the alignment-dependent ionization rate takes on a "peanut" shape which maximizes when the molecular axis is parallel to the polarization axis and minimizes when the molecular axis is perpendicular to the polarization axis. The laser intensity will strongly influence the overall ionization rate, and the ionization rate will increase dramatically with the increase of laser intensity. In Fig. 2(b) we show the same ionization rate, but normalized so that the maximum is unity for each laser intensity. The curves for different intensities almost overlap with each other, manifesting that the laser intensity has little effect on the alignment dependence of the ionization rate. In Fig. 2(c) we show the normalized ionization rate at different internuclear distances. We can see that the ionization rates for different internuclear distances differ significantly from each other. The minimum at perpendicular alignment gets smaller when the internuclear distance gets larger.

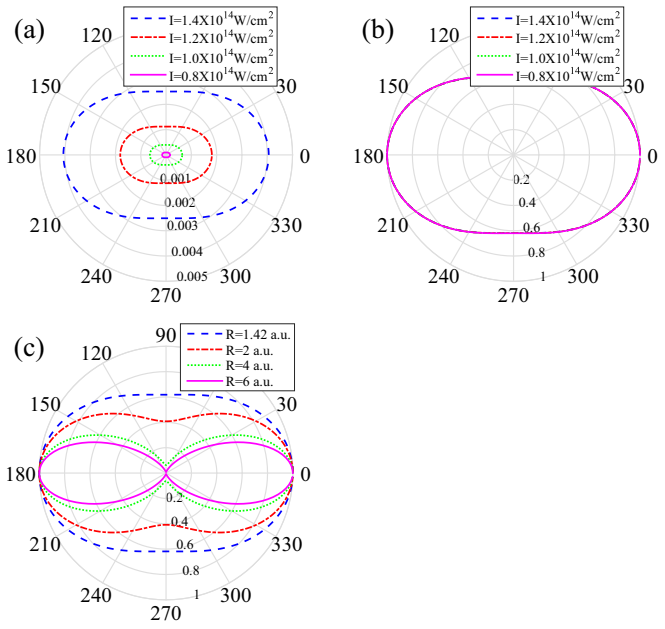

FIG. 2. (a) The alignment-dependent ionization rate of H_2 at equilibrium internuclear distance when the laser intensity is 1.4×10^{14} W/cm^2 (dashed blue line), 1.2×10^{14} W/cm^2 (dash-dotted red line), 1.0×10^{14} W/cm^2 (dotted green line), and 0.8×10^{14} W/cm^2 (solid magenta line). Because we neglect the coefficients in Eqs. (6) and (18), only the relative value among different curves is meaningful. (b) The same ionization rate as shown in (a), but normalized so that the maximum value for each intensity is unity. (c) Normalized ionization rate when the internuclear distance is 1.42 a.u. (dashed blue line, the equilibrium internuclear distance), 2 a.u. (dash-dotted red line), 4 a.u. (dotted green line), and 6 a.u. (solid magenta line).

The integral in Eq. (18) can be separated into three parts. From the derivation above we can see that the first two terms in the square brackets in Eq. (18) represent the ionization of two atoms without interfering with each other, and the third term represents two-center interference. In Fig. 3(a) we show the total ionization rate (dashed black line), and the contributions of atom 1 (dash-dotted blue line), atom 2 (dotted red line), and two-center interference (solid green line) at equilibrium internuclear distance. In Fig. 3(b) we show the corresponding result when $R = 4$ (a.u.). From Fig. 3(a) we can see that when the molecular axis is parallel to the polarization axis, the ionization of one of the two atoms is enhanced, and the other is suppressed [20], whereas when the molecular axis is perpendicular to the polarization axis, the two atoms contribute equally. The interference term is always positive, which reflects the bonding property of H_2 and will enhance the ionization. When increasing the internuclear distance, as shown in Fig. 3(b), the interference term decreases over all alignment angles, and one of the two atoms will dominate the distribution of corresponding side lobes.

IV. OXYGEN

The HOMO of O_2 is $1\pi_g$. In O_2 $\pi_g 2p_x$ and $\pi_g 2p_y$ orbitals are degenerate, and both orbitals have one electron with the same energy [21,22]. For clarity, here we present the treatment of the $\pi_g 2p_y$ orbital. As shown in Fig. 4(a), the $\pi_g 2p_y$ orbital is

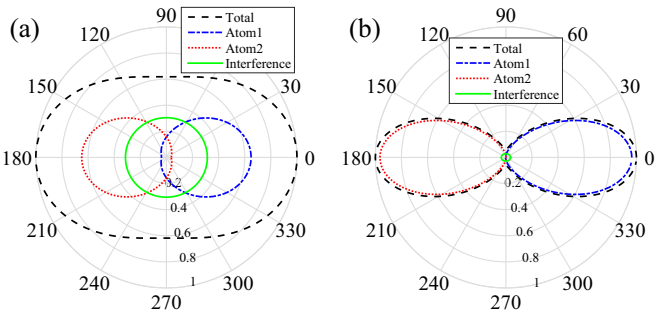

FIG. 3. (a) The total ionization rate (dashed black line) of H_2, and the contributions of atom 1 (dash-dotted blue line), atom 2 (dotted red line), and two-center interference (solid green line). H_2 is at equilibrium internuclear distance. The laser intensity is 1.2×10^{14} W/cm^2. (b) Same as (a) except that the internuclear distance is 4 a.u.

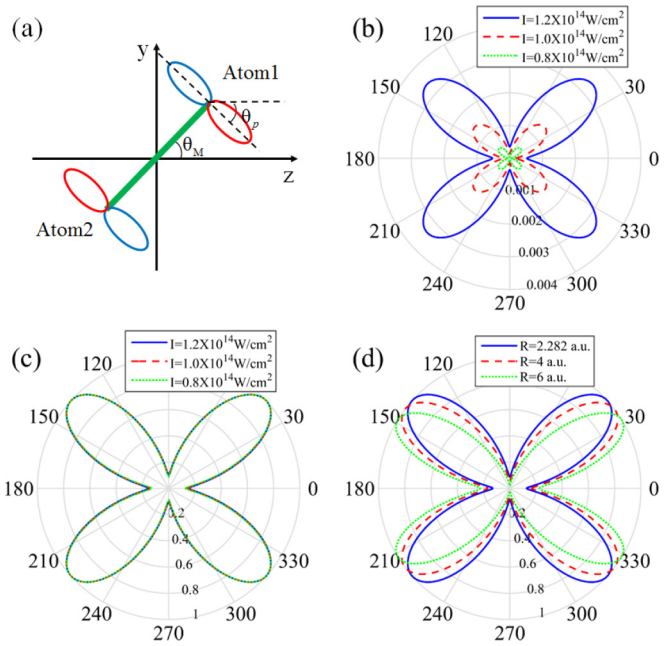

FIG. 4. (a) The configuration of O_2. The thick green line indicates the molecular axis. The alignment angle is θ_M. The dashed black lines indicate the orientation of the $2p_y$ orbital. The polar angle of the axis of symmetry of the $2p_y$ orbital is θ_p. (b) The alignment-dependent ionization rate of O_2 at equilibrium internuclear distance (2.282 a.u.) when the laser intensity is 1.2×10^{14} W/cm^2 (solid blue line), 1.0×10^{14} W/cm^2 (dashed red line), and 0.8×10^{14} W/cm^2 (dotted green line). (c) The same ionization rate as shown in (b), but normalized so that the maximum value for each intensity is unity. (c) Normalized ionization rate when the internuclear distance is 2.282 a.u. (solid blue line), 4 a.u. (dashed red line), and 6 a.u. (dotted green line).

the antibonding superposition of two $2p_y$ orbitals, one at each atomic center. Different from the $1s$ orbital, the $2p_y$ orbital is cylindrically symmetric, and we have to consider the orientation of the $2p_y$ orbital. We represent this orientation by the polar (θ_p) and azimuthal (φ_p) angles of the axis of symmetry of the $2p_y$ orbital. Because of the cylindrical symmetry of the $2p_y$ orbital, we do not need to consider the rotation around the axis of symmetry. Based on the description in Sec. II, an arbitrarily oriented $2p_y$ orbital can be represented as follows:

$$\Psi_{2p_y(\text{arb.ori.})}(\mathbf{r}) = \frac{1}{\sqrt{2}} \sin\theta_p e^{-i\varphi_p} \Psi_{211}(\mathbf{r}) - \frac{1}{\sqrt{2}} \sin\theta_p e^{i\varphi_p} \Psi_{21-1}(\mathbf{r}) - \cos\theta_p \Psi_{210}(\mathbf{r}). \tag{19}$$

The corresponding expression in mixed representation at tunnel exit is

$$\Phi_{2p_y(\text{arb.ori.})}(p_x,p_y,z_e) = \frac{1}{\sqrt{2}} \sin\theta_p e^{-i\varphi_p} \Phi_{211}(p_x,p_y,z_e) - \frac{1}{\sqrt{2}} \sin\theta_p e^{i\varphi_p} \Phi_{21-1}(p_x,p_y,z_e) - \cos\theta_p \Phi_{210}(p_x,p_y,z_e). \tag{20}$$

The expression of each atomic eigenstate can be given by Eqs. (9) and (13). After inserting the corresponding results into Eq. (20), we get the expression for an arbitrarily oriented $2p_y$ orbital,

$$\Phi_{2p_y(\text{arb.ori.})}(p_x,p_y,z_e) = \frac{C_{\kappa 0}}{\sqrt{\pi\, p_z(z_e)}} \frac{\sqrt{3}}{2} \left[\cos\theta_p - i\, \sin\theta_p \frac{p_\perp \cos(\varphi_p - \phi_0)}{\kappa}\right] \times \left(\frac{2\kappa^3}{F}\right)^{Q/\kappa} \exp\left(-\frac{\kappa^3}{3F} - \frac{\kappa p_\perp^2}{2F}\right). \tag{21}$$

Here the part in square brackets represents the effect of the structure and the orientation of the $2p_y$ orbital on the momentum distribution at tunnel exit.

As the HOMO of O_2 is the antibonding superposition of two $2p_y$ orbitals, one can give the expression in mixed representation straightforwardly, following the treatment of H_2. Note that the axis of symmetry of the $2p_y$ orbital is perpendicular to the molecular axis of O_2, thus only three of the four angles θ_M, φ_M, θ_p, and φ_p are independent. We make a further restriction that both the molecular axis and the axis of symmetry of $2p_y$ orbitals lie in the y-z plane; then the final expression is given by

$$\Phi_{O_2}(p_x,p_y,z_e) = \left\{\left[\exp(-i\,p_y R\, \sin\theta_M/2)\exp(\kappa R\, \cos\theta_M/2) - \exp(i\,p_y R\, \sin\theta_M/2)\exp(-\kappa R\, \cos\theta_M/2)\right] \times \left[\sin\theta_M + i\, \cos\theta_M \frac{p_y}{\kappa}\right]\right\} \times \frac{C_{\kappa 1}}{\sqrt{\pi\, p_z(z_e)}} \frac{\sqrt{3}}{2} \left(\frac{2\kappa^3}{F}\right)^{Q/\kappa} \exp\left(-\frac{\kappa^3}{3F} - \frac{\kappa p_\perp^2}{2F}\right) \tag{22}$$

From this expression, the structural factor is composed of two parts. The part in the first pair of square brackets originates from the displacement of corresponding atomic centers, and the part in the second pair of square brackets is the structural factor of the $2p_y$ orbital.

After inserting Eq. (22) into Eq. (16), we get the alignment-dependent ionization rate, as shown in Fig. 4. We can see that the overall ionization rate takes on a "flower" shape, consisting of four lobes [23]. Similar to the case of H_2, the laser intensity will change the overall ionization rate dramatically [see Fig. 4(b)], but has little effect on the alignment dependence [see Fig. 4(c)]. As shown in Fig. 4(d), the internuclear distance will change the alignment dependence significantly. The four lobes will bend towards the horizontal axis when we increase the internuclear distance.

Similar to the treatment of H_2, we separate the total ionization rate into three parts. In Fig. 5(a) we show the total ionization rate (dashed black line), and the contributions of atom 1 (dash-dotted blue line), atom 2 (dotted red line), and two-center interference (solid green line). Interestingly, the interference term is always negative, which reflects the antibonding property of the HOMO of O_2, and will decrease the overall ionization rate [24]. In Fig. 5(b) we show the sum of the contributions from two atoms without interference (dashed red line), which is much larger than the one including interference (solid blue line). The huge difference between the

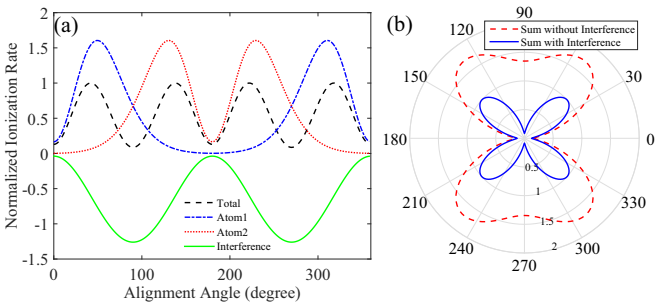

FIG. 5. (a) The total ionization rate (dashed black line) of O_2, and the contributions of atom 1 (dash-dotted blue line), atom 2 (dotted red line), and two-center interference (solid green line). O_2 is at equilibrium internuclear distance. The laser intensity is 0.8×10^{14} W/cm^2. The interference term is always negative, so we plot these curves in Cartesian coordinates. (b) The total ionization rate (solid blue line) and the sum of the contributions of atom 1 and atom 2 (dashed red line). The internuclear distance and laser intensity are the same as (a).

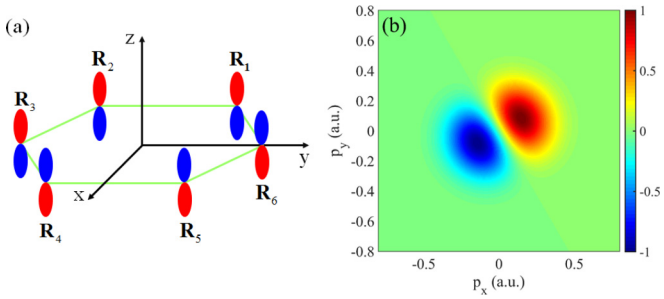

FIG. 6. (a) The sketch of the HOMO of benzene. Six carbon atoms constitute a hexagon lying in the x-y plane. The length of each side of this hexagon is 2.6267 a.u. There is one $2p$ orbital at each carbon atomic center, whose axis of symmetry is parallel to the z axis. Three of these $2p$ orbitals possess the same sign, and the other three possess an opposite sign. The ionization potential of benzene is 9.24 eV. The static electric field points towards minus z axis. (b) The momentum distribution at tunnel exit of benzene. The strength of the static electric field is 0.0228 a.u.

two curves in Fig. 5(b) manifests the significance of two-center interference in the ionization of O_2.

V. POLYATOMIC MOLECULE

As shown in Sec. II, the wave function in mixed representation at tunnel exit for homonuclear diatomic molecules is the coherent superposition of the contributions of two atomic centers. Thus, we can extend this approach to polyatomic molecules straightforwardly. The corresponding expression for a polyatomic molecule is the coherent superposition of the contributions of every atomic center. The coefficients of these contributions constitute the total structural factor, which encodes the information of the structure and the orientation of molecules.

Take benzene, for example. The HOMO of benzene is doubly degenerate. We consider one of the degenerate orbitals, which is the coherent superposition of six $2p$ orbitals, as shown in Fig. 6(a). Three of these $2p$ orbitals possess the same sign, and the other three possess an opposite sign. Following the same method as in previous sections, we give the expression of the wave function in mixed representation at tunnel exit of benzene:

$$\Phi_{C_6H_6}(p_x,p_y,z_e) = \left\{ \begin{bmatrix} +\exp(-i\,p_x x_1 - i\,p_y y_1)\exp(\kappa z_1) \\ +\exp(-i\,p_x x_2 - i\,p_y y_2)\exp(\kappa z_2) \\ +\exp(-i\,p_x x_3 - i\,p_y y_3)\exp(\kappa z_3) \\ -\exp(-i\,p_x x_4 - i\,p_y y_4)\exp(\kappa z_4) \\ -\exp(-i\,p_x x_5 - i\,p_y y_5)\exp(\kappa z_5) \\ -\exp(-i\,p_x x_6 - i\,p_y y_6)\exp(\kappa z_6) \end{bmatrix} \left[\cos\theta_p - i\,\sin\theta_p \frac{p_\perp \cos(\varphi_p - \phi_0)}{\kappa} \right] \right\} \times \frac{C_{\kappa 0}}{\sqrt{\pi}\,p_z(z_e)} \frac{\sqrt{3}}{2} \left(\frac{2\kappa^3}{F} \right)^{Q/\kappa} \exp\left(-\frac{\kappa^3}{3F} - \frac{\kappa p_\perp^2}{2F} \right) \tag{23}$$

Here (x_i, y_i, z_i), $i = 1,2,\ldots,6$ are the positions of six carbon atomic centers, respectively. Note that the six carbon atomic centers lie in the same plane, which is perpendicular to the axis of symmetry of the $2p$ orbital. Similar to the result of O_2, the expression in the curly braces is the total structural factor. It is composed of two parts. The part in the first pair of square brackets is composed of six exponential terms, and each of them corresponds to the contribution of one atomic center. The positive or negative sign before each term represents the sign of the corresponding $2p$ orbital. The part in the second pair of square brackets represents the effect of the structure and the orientation of the $2p$ orbital, as the expression in Eq. (21). For the specific configuration in Fig. 6(a), we show the result of Eq. (23) in Fig. 6(b), which also represents the two-dimensional transverse momentum distribution at tunnel exit. We can see that the distribution is composed of two parts, and a clear nodal structure originates from the interference between three positive $2p$ orbitals and three negative $2p$ orbitals. The wave function changes its sign across the nodal structure, which represents a phase jump of π at this specific configuration. The position of the nodal structure depends on the configuration of the molecule, and if we rotate the molecule, the nodal structure will rotate accordingly.

VI. CONCLUSION

We present a straightforward method to calculate the strong-field ionization of aligned molecules, based on the

combination of the partial-Fourier-transform approach and WKB approximation, which possesses the capacity to deal with homonuclear diatomic molecules, as well as polyatomic molecules. We calculate the alignment-dependent ionization rate of homonuclear diatomic molecules, and show that the internuclear distance has a significant effect on the alignment dependence of ionization rate. Different from the MO-ADK theory, with the present method we can separate the contributions of each atom and show the interference effect between them. We obtain the analytical expression of the momentum distribution at tunnel exit, which can be regarded as the initial conditions of semiclassical simulations [25] to calculate the photoelectron momentum distribution of aligned diatomic and polyatomic molecules [18]. We point out that the method in present form is applied to the stationary tunneling problem, which necessitates the use of a length gauge. It is possible to generalize this method to the study of nonstationary problems if the classical action under the barrier in an alternating field is considered [26].

ACKNOWLEDGMENTS

This work is supported by the National Program on Key Basic Research Project (Grant No. 2013CB922403) and the National Science Foundation of China (Grants No. 11434002 and No. 11125416).

[1] P. B. Corkum, Phys. Rev. Lett. **71**, 1994 (1993).
[2] J. Itatani, J. Levesque, D. Zeidler, H. Niikura, H. Pépin, J. C. Kieffer, P. B. Corkum, and D. M. Villeneuve, Nature (London) **432**, 867 (2004).
[3] M. Meckel, D. Comtois, D. Zeidler, A. Staudte, D. Pavičić, H. C. Bandulet, H. Pépin, J. C. Kieffer, R. Dörner, D. M. Villeneuve, and P. B. Corkum, Science **320**, 1478 (2008).
[4] M. Meckel, A. Staudte, S. Patchkovskii, D. M. Villeneuve, P. B. Corkum, R. Dörner, and M. Spanner, Nat. Phys. **10**, 594 (2014).
[5] J. Xu, C. I. Blaga, K. Zhang, Y. H. Lai, C. D. Lin, T. A. Miller, P. Agostini, and L. F. DiMauro, Nat. Commun. **5**, 4635 (2014).
[6] M. G. Pullen, B. Wolter, A.-T. Le, M. Baudisch, M. Hemmer, A. Senftleben, C. D. Schroter, J. Ullrich, R. Moshammer, C. D. Lin, and J. Biegert, Nat. Commun. **6**, 7262 (2015).
[7] L. V. Keldysh, Zh. Eksp. Teor. Fiz. **47**, 1945 (1964) [Sov. Phys. JETP **20**, 1307 (1965)].
[8] S. V. Popruzhenko, J. Phys. B **47**, 204001 (2014).
[9] A. M. Perelomov, V. S. Popov, and M. V. Terent'ev, Zh. Eksp. Teor. Fiz. **50**, 1393 (1966) [Sov. Phys. JETP **23**, 924 (1966)].
[10] M. V. Ammosov, N. B. Delone, and V. P. Krainov, Zh. Eksp. Teor. Fiz. **91**, 2008 (1986) [Sov. Phys. JETP **64**, 1191 (1986)].
[11] G. L. Yudin and M. Yu. Ivanov, Phys. Rev. A **64**, 013409 (2001).
[12] D. B. Milošević, Phys. Rev. A **74**, 063404 (2006).
[13] M. Busuladžić, A. Gazibegović-Busuladžić, D. B. Milošević, and W. Becker, Phys. Rev. A **78**, 033412 (2008).
[14] M. Busuladžić, A. Gazibegović-Busuladžić, and D. B. Milošević, Phys. Rev. A **80**, 013420 (2009).
[15] X. M. Tong, Z. X. Zhao, and C. D. Lin, Phys. Rev. A **66**, 033402 (2002).
[16] R. Murray, W.-K. Liu, and M. Yu. Ivanov, Phys. Rev. A **81**, 023413 (2010).
[17] R. Murray, M. Spanner, S. Patchkovskii, and M. Yu. Ivanov, Phys. Rev. Lett. **106**, 173001 (2011).
[18] M.-M. Liu, M. Li, C. Wu, Q. Gong, A. Staudte, and Y. Liu, Phys. Rev. Lett. **116**, 163004 (2016).
[19] A. M. Perelomov and V. S. Popov, Zh. Eksp. Teor. Fiz. **52**, 514 (1967) [Sov. Phys. JETP **25**, 336 (1967)].
[20] A. Staudte, S. Patchkovskii, D. Pavicic, H. Akagi, O. Smirnova, D. Zeidler, M. Meckel, D. M. Villeneuve, R. Dorner, M. Yu. Ivanov, and P. B. Corkum, Phys. Rev. Lett. **102**, 033004 (2009).
[21] V. I. Usachenko and Shih-I Chu, Phys. Rev. A **71**, 063410 (2005).
[22] D. A. McQuarrie and J. D. Simon, *Physical Chemistry: A Molecular Approach* (University Science Books, Sausalito, CA, 1997).
[23] D. Pavicic, K. F. Lee, D. M. Rayner, P. B. Corkum, and D. M. Villeneuve, Phys. Rev. Lett. **98**, 243001 (2007).
[24] J. Muth-Böhm, A. Becker, and F. H. M. Faisal, Phys. Rev. Lett. **85**, 2280 (2000).
[25] M. Li, J.-W. Geng, H. Liu, Y. Deng, C. Wu, L.-Y. Peng, Q. Gong, and Y. Liu, Phys. Rev. Lett. **112**, 113002 (2014).
[26] M. Li, J.-W. Geng, M. Han, M. M. Liu, L.-Y. Peng, Q. Gong, and Y. Liu, Phys. Rev. A **93**, 013402 (2016).